Asian Journal of Chemistry; Vol. 37, No. 12 (2025), 3111-3115
ASIAN JOURNAL OF CHEMISTRY
https://doi.org/10.14233/ajchem.2025.34754

Synthesis of (0.5-9 mol%) Pr^{3+} doped MgO Nanoparticle for Display and Latent Fingerprints Application

R. VIJAY KUMAR[1], H.J. AMITH YADAV[1,*], B. ERAIAH[2], S. RAJENDRA PRASAD[3], SUSHMA KATTI[1], V.S. VEENA[1,4] and YASHWANTH VENKATRAMAN NAIK[5]

[1]Department of Studies in Physics, Davangere University, Davangere-577007, India
[2]Department of Physics, Bangalore University, Bangalore-560056, India
[3]Department of Chemistry, Davangere University, Davangere-577007, India
[4]Department of Physics, Government First Grade College, Koratagere-572129, India
[5]Department of Physics, RV Institute of Technology and Management, Bangalore-560076, India

*Corresponding author: E-mail: amithyadavhj@gmail.com

Received: 24 August 2025 *Accepted*: 22 October 2025 *Published online*: 30 November 2025 AJC-22202

Pr^{3+} (0.5-9 mol%) doped MgO nanoparticles were successfully synthesized *via* a solution combustion method using aloe vera gel as a green fuel. The powder X-ray diffraction (PXRD) patterns confirmed the formation of a single-phase cubic structure for all compositions. The morphological characteristics of the synthesized nanoparticles were investigated using microscopic techniques. The optical energy band gap (E_g), estimated from UV–visible absorption spectra, was found to vary from 5.06 to 5.59 eV with increasing Pr^{3+} concentration. Photoluminescence (PL) excitation spectra recorded in the 350–800 nm range revealed characteristic emissions and the corresponding CIE chromaticity coordinates were located in the blue-green region. These results suggest that the developed phosphor materials are promising candidates for use as blue-green components in white light-emitting devices. Furthermore, Pr^{3+} (1 mol%) doped MgO nanoparticles demonstrated excellent performance in visualizing latent fingerprints (LFPs) on glass surfaces, indicating their potential application in forensic science.

Keywords: Combustion method, Display application, Latent fingerprint application.

INTRODUCTION

Magnesium oxide (MgO) material in nanosize forms have various applications in catalysis, toxic waste remediation, refractory, translucent ceramics, paint, superconductors, absorbents, *etc*. [1-3]. The optical properties of MgO nanoparticles depend mainly on the intrinsic stability, wide bandgap, crystal lattice and defects [4]. It is important to know the size-dependent properties of MgO nanoparticle due to various applications in the field of nanoscience and technology. Numerous methods such as the wet chemical [5], sol-gel [6], microwave synthesis [7], precipitation [8] and hydrothermal process [9] have been used to synthesis MgO nanoparticles. However, these methods usually require expensive equipment, high temperature and multiple steps. On the contrary, combustion synthesis seems attractive due to their low cost, rapid and energy-efficient synthesis [10].

Generally, doping involves incorporation of foreign elements into a host material altering the optical and electrical properties of the MgO nanoparticle. Rare-earth (RE) doped MgO nanoparticles has received great attention due to the optical properties originating from the 4*f* transitions [11]. In the lanthanide series, Pr^{3+} ions doped metal oxide attracted the attention due to their red and green-blue emissions property [12,13].

In recent years, white light emitting diodes (WLEDs) is replacing incandescence bulb due to its low cost, high output, environmental benignity and long lifetime [14]. The intense and sharp emissions peak of praseodymium in its trivalent form could support the display application [15,16]. According to the literature, there are only a limited number of studies on Pr^{3+}- doped magnesium oxide (MgO) nanoparticles [17]. For this reason, we intend to study the luminescence properties of Pr-dopant on the optical properties of MgO nanoparticles.

Moreover, rare earth doped metallic oxide nanoparticles, with their strong luminescence and high surface area due to their unique morphology, present a promising material for latent finger-print detection [18,19]. The intense photoluminescence emission enables clear visualization of fingerprint ridges and pores under UV illumination, improving the contrast between the fingerprint residue and background surfaces [20]. The nanoscale size and porous nature of doped materials facilitate better adhesion to sweat pore secretions, allowing enhanced detection of fine details such as sweat pores [20,21]. Thus, the luminescent properties combined with the physical characteristics of Pr^{3+}-doped MgO nanoparticles make them highly suitable for dual applications in both optoelectronic displays and sensitive forensic fingerprint imaging.

Herein, we have reported a green synthesis of Pr^{3+} (0.5-9 mol%) doped MgO nanoparticles using aloe-vera gel as fuel. The advantages of plant mediated fuels are low cost, less toxic, eco-friendly, high homogeneity, high crystallinity and good phase purity [22,23]. Furthermore, the synthesized doped materials were explored for their practical application in the visualization of latent fingerprints (LFPs) on glass surfaces, demonstrating their potential in forensic investigations.

EXPERIMENTAL

The chemicals, magnesium nitrate, praseodymium nitrate hexahydrate ($Pr(NO_3)_3{\cdot}6H_2O$) as precursors, were procured from Merck (USA). X-ray diffraction (XRD) patterns were recorded using a Bruker D8 Advance diffractometer with Cu*K*α radiation (λ = 1.5406 Å). The surface morphology of the samples was examined using a field emission scanning electron microscope (FESEM, Carl Zeiss Supra 55). UV-Vis spectroscopy was carried out with an Agilent Technologies Cary Eclipse spectrophotometer. Photoluminescence (PL) spectra were recorded using a Perkin-Elmer Fluorescence Spectrophotometer (FL5600) equipped with a double-grating monochromator and a xenon lamp as the excitation source.

Synthesis of MgO:Pr^{3+} (0.5-9 mol%) nanoparticles: Pr^{3+} (0.5-9 mol%) doped MgO nanoparticles was successfully prepared by combustion method using aloe vera gel as fuel. The stoichiometric amount of $Mg(NO_3)_2$, $Pr(NO_3)_3{\cdot}6H_2O$ and aloe vera gel were dissolved in distilled water with constant stirring and then this reaction mixture was preheated in muffle furnace at 500 ± 5 ºC. The resultant product was formed within 5 min and then annealed at 700 ºC in the muffle furnace for 2 h.

RESULTS AND DISCUSSION

PXRD studies: Crystal structure of MgO nanoparticles with varied concentrations of Pr^{3+} (0.5-9 mol%) were characterized using PXRD and matched with standard JCPDS card No. 87-0653 as shown in Fig. 1. PXRD pattern confirms the cubic phase of MgO nanoparticles [24,25].

UV-Vis studies: The optical spectra of Pr^{3+} (0.5-9 mol%) doped MgO composites in the range of 100-600 nm wavelengths is shown in Fig. 2a. The optical absorption of the five samples show a strong absorption around 220-275 nm and the absorption edge is shifted to lower wavelength upon Pr^{3+} doped MgO [26]. The values of band gap for (0.5-9 mol%) Pr^{3+}-doped MgO nanoparticles calculated by the Tauc plots (Fig. 2b) found to be in range 5.06 to 5.59eV [27].

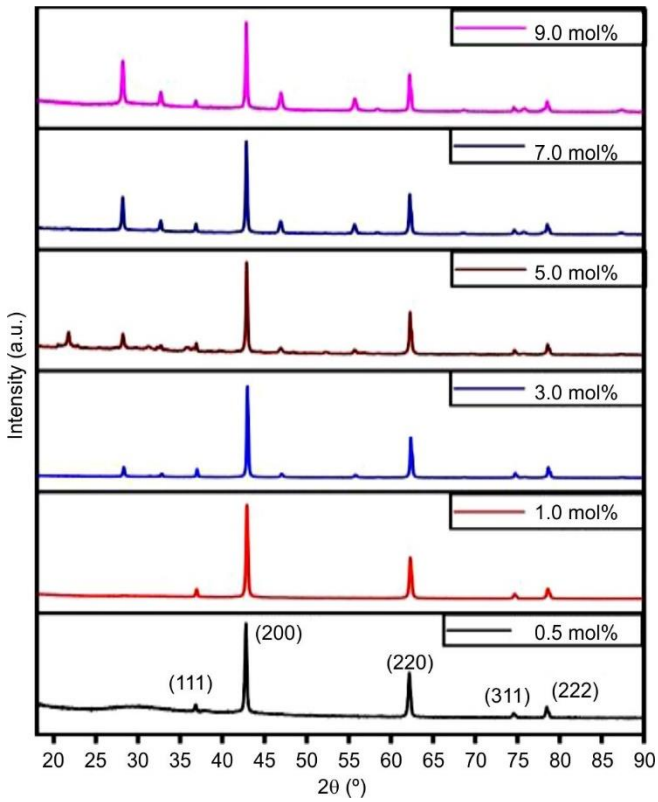

Fig. 1. PXRD patterns of Pr^{3+} (0.5-9 mol%) doped MgO nanoparticles

Surface morphology: Fig. 3 displays the SEM micrograph of the MgO nanophosphor doped with 1 mol% Pr^{3+} ions. The image shows that the particles have an uneven and irregular morphology, consisting mainly of thin, plate-like formations with curled and slightly folded edges. This structural appearance suggests that the inclusion of Pr^{3+} ions during syn-thesis may have influenced the particle growth, leading to partial aggregation and surface distortion. Small pores and voids can also be observed among the particles, indicating a loosely packed structure. Such features are likely to increase the effective surface area of the material and may play a significant role in modifying its optical and luminescent behaviour.

Photoluminescence (PL) studies: As PL was a surface phenomenon, then smoother surface gives better emission, as related to the coarser one [28]. Excitation spectra of Pr^{3+} (0.5-9 mol%) doped MgO nanoparticles recorded at 468 nm emission wavelength as shown in Fig. 4a. Fig. 4a shows that one intense sharp peak at 376 nm [29]. The emission peaks of Pr^{3+} (0.5-9 mol%) doped MgO nanoparticles recorded at excitation wavelength 376 nm as shown in Fig. 4b. From Fig. 4b, it is observed that one cyan emission peak at 492 nm ($^3P_0 \rightarrow {}^3H_4$). The radiative depopulation of the $^3P_0$ state gives rise to emission bands in the red region of the spectrum, including transitions from $^3P_0 \rightarrow {}^3F_2$ at 663 nm, $^3P_0 \rightarrow {}^3F_4$ at 764 nm.

Fig. 4b also shows that the emission peak at 468 nm exhibits a higher intensity compared to the other peaks, which can be attributed to the strong population of the $^3P_1$ excited

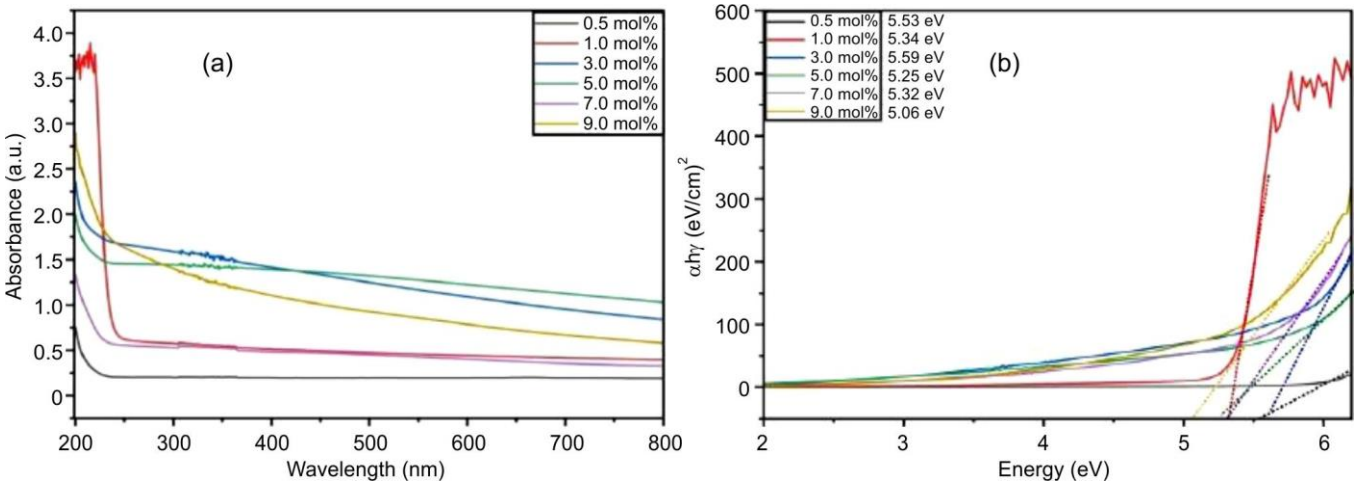

Fig. 2. (a) Absorption spectra of Pr^{3+} (0.5-9 mol%) doped MgO samples, (b) the Tauc plots given band gaps

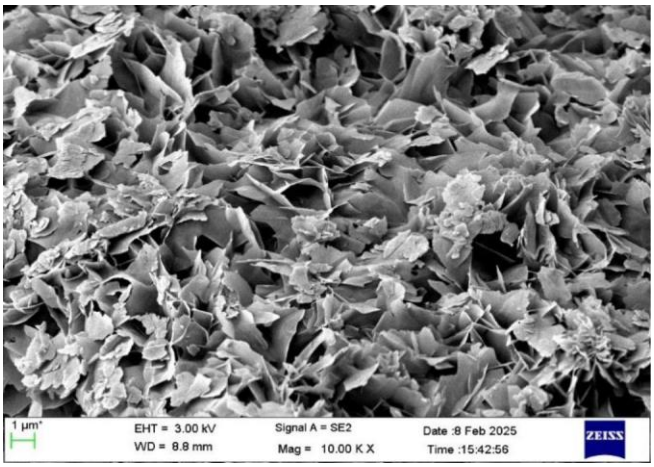

Fig. 3. SEM image of Pr^{3+} (1 mol%) doped MgO nanoparticles

state [30]. The optimal concentration of Pr^{3+} ions in MgO nanoparticles was also investigated to determine its effect on luminescence behaviour. As observed in Fig. 4c, the photoluminescence (PL) emission intensity initially increases with Pr^{3+} doping and reaches its maximum at 1 mol%. Beyond this concentration, the emission intensity gradually decreases due to concentration quenching, which occurs as a result of non-radiative energy transfer among adjacent Pr^{3+} ions [12]. Fig. 4d illustrates the energy-level diagram of Pr^{3+} ions, demonstrating the possible electronic transitions responsible for the observed blue-green emission.

Colour parameters: Fig. 5 presents the Commission Internationale de l'Éclairage (CIE) chromaticity diagram for MgO nanoparticles doped with varying concentrations of Pr^{3+} ions (1–9 mol%). The emission coordinates for each concentration were derived from the PL spectra, and the corresponding CIE and correlated colour temperature (CCT) values are summarized in Tables 1 and 2, respectively. As illustrated in Fig. 5, the emission points are primarily located in the blue-green region of the chromaticity diagram, confirming that the dominant emission arises from electronic transitions within the Pr^{3+} ion energy levels, particularly from the $^3P_1 \rightarrow {}^3H_5$, transition. The slight shift in chromaticity coordinates with increasing dopant concentration suggests minor variations in

TABLE-1
THE CIE COORDINATES OF MgO:Pr^{3+} (0.5-9 mol%) NANOPARTICLES

	x	y
0.5 mol%	0.28200	0.30463
1.0 mol%	0.27204	0.29619
3.0 mol%	0.27707	0.30859
5.0 mol%	0.28663	0.31209
7.0 mol%	0.24474	0.22955
9.0 mol%	0.26856	0.28640

TABLE-2
THE CCT COORDINATES OF MgO:Pr^{3+} (0.5-9 mol%) NANOPARTICLES

	u'	v'	CCT
0.5 mol%	0.1852	0.4501	9061
1.0 mol%	0.1811	0.4435	10360
3.0 mol%	0.1802	0.4517	9333
5.0 mol%	0.1858	0.4551	8456
7.0 mol%	0.1859	0.3924	36934
9.0 mol%	0.1821	0.4369	11366

the local crystal field environment and energy transfer efficiency among Pr^{3+} ions. These observations indicate that Pr^{3+}-doped MgO nanophosphors can effectively emit in the blue-green spectral region, making them suitable candidates for display and optoelectronic applications.

Forensic application: In this study, latent fingerprints (LFPs) from a healthy individual were deposited on glass surfaces. The micrographs (Fig. 6) demonstrate that the use of 1 mol% Pr^{3+}-doped MgO nanoparticles enables clear visualization of the fingerprint ridges, significantly enhancing the contrast compared to untreated fingerprints [31]. Importantly, the nanoparticles allow the observation of all three levels of fingerprint as (i) the overall ridge patterns such as loops (Level I), (ii) minutiae including dots, bifurcations and bridges (Level II); and (iii) individual sweat pores (Level III). This enhanced visualization can be attributed to the strong blue-green luminescence of the Pr^{3+}-doped MgO nanoparticles, which effectively adhere to the fingerprint residues and emit under UV illumination, revealing fine structural details that are critical for high-accuracy forensic identification.

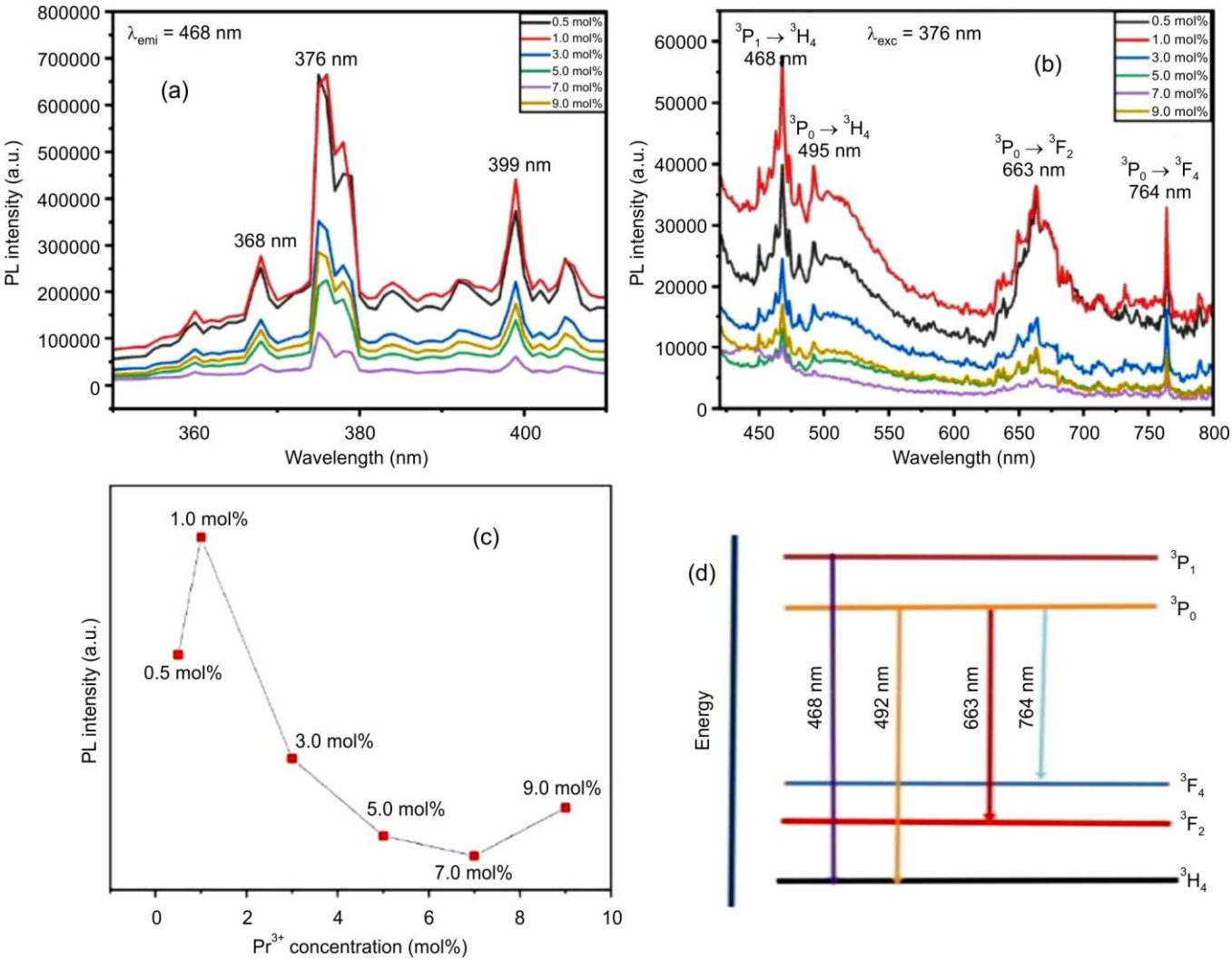

Fig. 4. (a) Excitation spectrum, (b) emission spectra, (c) PL intensity *versus* Pr^{3+} conc and (d) energy level diagram of Pr^{3+} ions

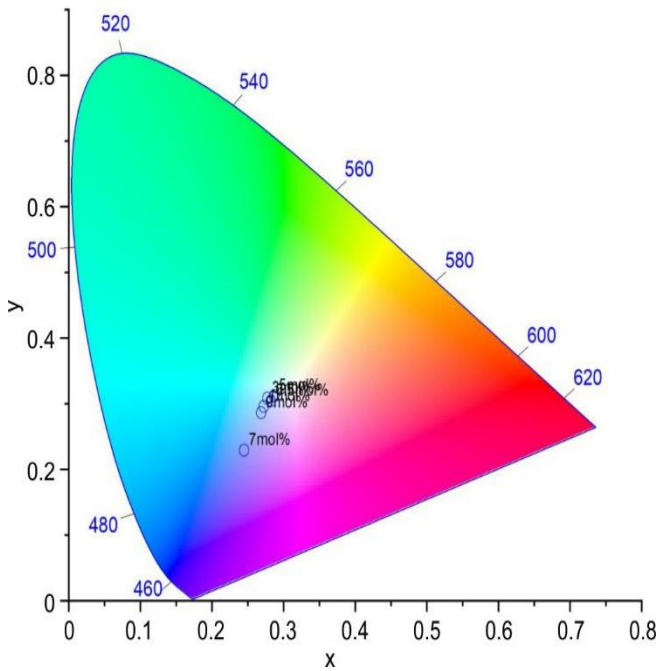

Fig. 5. CIE coordinates of Pr^{3+} (0.5-9 mol%) doped MgO nanoparticles

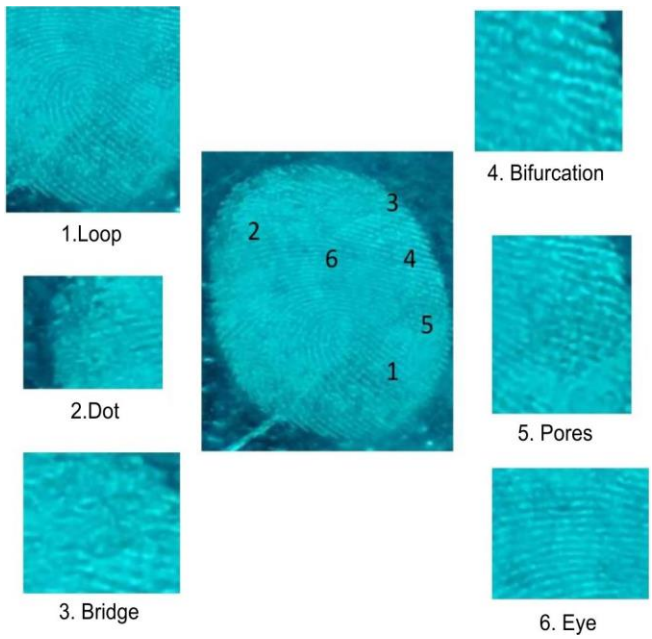

Fig. 6. Latent fingerprints (LFPs) visualized by staining Pr^{3+} (1 mol%) doped MgO nanoparticles

Conclusion

In this work, Pr^{3+} (0.5-9 mol%) doped MgO nanoparticles were successfully synthesized and characterized for the structural, optical and luminescent properties, as well as forensic applications. PXRD confirmed the cubic structure of MgO, while SEM revealed irregular, plate-like, porous morphologies enhancing surface area and optical interactions. UV-Vis and PL studies showed strong blue-green emission, with maximum intensity at 1 mol% Pr^{3+}, and a band gap range of 5.06-5.59 eV. CIE analysis confirmed blue-green emission suitable for display and optoelectronic applications. For forensic evaluation, 1 mol% Pr^{3+}-doped MgO nanoparticles enabled clear visualization of all three levels of latent fingerprint detail including ridge patterns, minutiae, and sweat pores under UV illumination, due to strong luminescence and effective adhesion to fingerprint residues. These results demonstrate that Pr^{3+}-doped MgO nanoparticles are promising multifunctional materials for both optoelectronic devices and high-resolution latent fingerprint detection.

ACKNOWLEDGEMENTS

The authors acknowledge Vision Group on Science and Technology (VGST), Government of Karnataka, India [VGST /GRD-1178] for sanction of the project. The authors also acknowledge the facilities provided by USIC, Davangere University, Davangere and Centre for Excellence in Advanced Materials Research, Department of Physics (SoAS), REVA University, Bangalore, India for the characterization of the samples.

CONFLICT OF INTEREST

The authors declare that there is no conflict of interests regarding the publication of this article.

REFERENCES

1. A.J. Kadham, D. Hassan, N. Mohammad and A.H. Ah-Yasari, *Bull. Electr. Eng. Informatics*, **7**, 28 (2018); https://doi.org/10.11591/eei.v7i1.839
2. A. Hashim and A. Hadi, *Sens. Lett.*, **15**, 858 (2017); https://doi.org/10.1166/sl.2017.3900
3. J. Hornak, *Int. J. Mol. Sci*., **22**, 12752 (2021); https://doi.org/10.3390/ijms222312752
4. P. Saengkwamsawang and K. Tochat, *J. Nanopart. Res.*, **23**, 214 (2021); https://doi.org/10.1007/s11051-021-05323-0
5. Q.-W. Liu, S.-J. Guo, M.-Y. Qi and A.-M. Cao, *Chem. Commun.*, **61**, 298 (2024); https://doi.org/10.1039/D4CC05626D
6. A.C. Gurule, S.S. Gaikwad, D.D. Kajale, V.S. Shinde, G.R. Jadhav and V.B. Gaikwad, *J. Indian Chem. Soc.*, **102**, 101496 (2025); https://doi.org/10.1016/j.jics.2024.101496
7. S. Wei, Y. Tao, M. Ma, W. Tong, F. Bi, L. Wang, J. Qu and Y. Zhang, *Sep. Purif. Technol.*, **354**, 128936 (2025); https://doi.org/10.1016/j.seppur.2024.128936
8. S. Chen and H.H. Yun, *Surf. Innov.*, **13**, 84 (2025); https://doi.org/10.1680/jsuin.24.00103
9. A.R. Safira, A. Fattah-alhosseini, M. Alkaseem and M. Kaseem, *J. Magnesium Alloys*, **13**, 1203 (2025); https://doi.org/10.1016/j.jma.2025.02.001
10. A. Kumar, M. Balakrishna, U. Desai, R. Rakshith, K.M. Ambika, P. Soumya, C.R. Ravikumar, S.S. Vadivu and N. Naik, *Sci. Rep.*, **15**, 338 (2025); https://doi.org/10.1038/s41598-024-82764-2
11. M.K. Hossain, S. Hossain, M.H. Ahmed, M.I. Khan, N. Haque and G.A. Raihan, *ACS Appl. Electron. Mater*., **3**, 3715 (2021); https://doi.org/10.1021/acsaelm.1c00682
12. R.B. Basavaraj, D. Navami, N.H. Deepthi, M. Venkataravanappa, R. Lokesh, K.H. Sudheer Kumar and T.K. Sreelakshmi, *Inorg. Chem. Commun.*, **120**, 108164 (2020); https://doi.org/10.1016/j.inoche.2020.108164
13. L. Yu, J. Hao, W. Li, P. Fu, W. Sun, C. Chen, Z. Xu and R. Chu, *J. Mater. Sci. Mater. Electron.*, **30**, 17890 (2019); https://doi.org/10.1007/s10854-019-02141-y
14. B. Shao, J. Huo and H. You, *Adv. Opt. Mater.*, **7**, 1900319 (2019); https://doi.org/10.1002/adom.201900319
15. J.H. Oh, Y.J. Eo, H.C. Yoon, Y.-D. Huh and Y. R. Do, *J. Mater. Chem. C*, **36**, 8326 (2016); https://doi.org/10.1039/C6TC02387H
16. L. Renuka, K.S. Anantharaju, S.C. Sharma, H.P. Nagaswarupa, S.C. Prashantha, H. Nagabhushana and Y.S. Vidya, *J. Alloys Compd*., **672**, 609 (2016); https://doi.org/10.1016/j.jallcom.2016.02.124
17. T. Suemoto, T. Okuno and D. Nakano, *Opt. Commun*., **145**, 113 (1998); https://doi.org/10.1016/S0030-4018(97)00496-3
18. B.N. Swathi, B.R. Radha, K. Krishtappa Manjunatha, W.-C. Lo, T.-E. Hsu, C.-Y. Jheng, M.-K. Ho, H.-H. Chiu, S.-L. Yu, Y.-L. Huang, S.C. Sharma, B. Subramanian, S.Y. Wu and H. Nagabhushana, *ACS Appl. Nano Mater*., **6**, 21322 (2023); https://doi.org/10.1021/acsanm.3c04699
19. R.K. Jain, S.N. Ananya, P.J. Anand and D. Sunil, *Microchem. J*., **209**, 112749 (2025): https://doi.org/10.1016/j.microc.2025.112749
20. S. Atri, K. Verma, B. Joshi and S. Kataria, *J. Radiat. Res. Appl. Sci.*, **18**, 101225 (2025); https://doi.org/10.1016/j.jrras.2024.101225
21. A. Sharma, M. S. Sankhla, S. S. Bhati, A. Agrawal and S. Tyagi, *Discover Nano*, **20**, 175 (2025); https://doi.org/10.1186/s11671-025-04317-4
22. N.T. Tran, K.L. Nguyen, G.T. Nguyen, A.T.N. Huynh and T.M. Le, *Colloid Polym. Sci.*, **303**, 1189 (2025); https://doi.org/10.1007/s00396-025-05410-x
23. H.J. Amith Yadav, B. Eraiah, H. Nagabhushana, G.P. Darshan, B. Daruka Prasad, M.K. Sateesh, S.C. Sharma and P.H. Prabha, *J. Sci. Adv. Mater. Devices*, **2**, 455 (2017); https://doi.org/10.1016/j.jsamd.2017.11.004
24. P. Vanishree and G. Swati, *J. Mater. Sci.: Mater. Electr*., **35**, 597 (2024); https://doi.org/10.1007/s10854-024-12350-9
25. P.A. Prathap, H.S. Bhojya Naik, R. Viswanath, N. Adarshgowda, G. Vishnu and K.R. Kotresh, *Chem. Data Coll*., **51**, 101131 (2024); https://doi.org/10.1016/j.cdc.2024.101131
26. S. Narendhran, M. Manikandan and P.B. Shakila, *Bull. Mater. Sci.*, **42**, 133 (2019); https://doi.org/10.1007/s12034-019-1811-7
27. E.I. Naik, H.S.B. Naik, B.E.K. Swamy, R. Viswanath, I.K.S. Gowda, M.C. Prabhakara and K. Chetankumar, *Chem. Data Coll.*, **33**, 100671 (2021); https://doi.org/10.1016/j.cdc.2021.100671
28. Q. Zhu, J.-G. Li, X. Li and X. Sun, *Acta Mater.*, **57**, 5975 (2009); https://doi.org/10.1016/j.actamat.2009.08.026
29. S. Tomar, N. K. Mishra, V. Chauhan, K. Kumar and C. Shivakumara, *Dalton Trans.*, **54**, 1913 (2025); https://doi.org/10.1039/D4DT02532F
30. W. Shi, J. Du, Y. Zhai, C. Chen, Y. Wei, W. Li, J. Hao and P. Fu, *J. Mater. Sci.*, **55**, 5741 (2020); https://doi.org/10.1007/s10853-020-04444-6
31. D. Navami, R.B. Basavaraj, S.C. Sharma, B. Daruka Prasad and H. Nagabhushana, *J. Alloys Compd.*, **762**, 763 (2018); https://doi.org/10.1016/j.jallcom.2018.05.016